

Beam energy dependence of pseudorapidity distributions of charged particles produced in heavy-ion collisions at RHIC and LHC energies

Sumit Basu and Tapan K. Nayak
Variable Energy Cyclotron Centre, Kolkata 700064, India

Kaustuv Datta
Department of Physics, Reed College, Portland, OR 97202, USA
(Dated: May 2, 2016)

Heavy-ion collisions at the Relativistic Heavy Ion Collider at Brookhaven National Laboratory and the Large Hadron Collider at CERN probe matter at extreme conditions of temperature and energy density. Most of the global properties of the collisions can be extracted from the measurements of charged particle multiplicity and pseudorapidity (η) distributions. We have shown that the available experimental data on beam energy and centrality dependence of η -distributions in heavy-ion (Au+Au or Pb+Pb) collisions from $\sqrt{s_{NN}} = 7.7$ GeV to 2.76 TeV are reasonably well described by the AMPT model, which is used for further exploration. The nature of the η -distributions has been described by a double Gaussian function using a set of fit parameters, which exhibit a regular pattern as a function of beam energy. By extrapolating the parameters to a higher energy of $\sqrt{s_{NN}} = 5.02$ TeV, we have obtained the charged particle multiplicity densities, η -distributions and energy densities for various centralities. Incidentally, these results match well with some of the recently published data by the ALICE collaboration.

PACS numbers: 25.75.-q, 25.75.Dw, 24.10.Lx, 12.38.Mh

I. INTRODUCTION

The primary goal of colliding heavy-ions at ultra-relativistic energies is to study nuclear matter under extreme conditions, in which hadronic matter is expected to undergo a phase transition to a new state of matter, the Quark-Gluon Plasma (QGP) [1, 2]. Quantum Chromodynamics (QCD), the theory of strong interactions, suggests that at high temperatures and energy densities, nuclear matter melts down to this new phase of deconfined quarks and gluons. Recent Lattice QCD calculations [3, 4] indicate that transition from hadronic matter to QGP occurs at a critical temperature of $T_C \sim 155$ MeV and critical energy density of $\epsilon_C \sim 0.7 - 1.9$ GeV/fm³. The QGP research programs at the Relativistic Heavy Ion Collider (RHIC) at Brookhaven National Laboratory and the Large Hadron Collider (LHC) at CERN are on a quest to unearth the physics of deconfinement and vacuum, and to understand how matter behaved within a few microseconds after the birth of our Universe. With the first phase of the beam energy scan program at RHIC during 2010 and 2011, data for Au+Au collisions at a nucleon-nucleon (NN) centre-of-mass energy ($\sqrt{s_{NN}}$) from 7.7 GeV to 200 GeV are available. The main aim of this program is to probe the onset of deconfinement and to locate the QCD Critical Point [5]. The LHC has collided Pb+Pb beams at $\sqrt{s_{NN}} = 2.76$ TeV during the first phase of its operation (2010 and 2011). During the first year of the second phase of LHC operation in 2015, data for Pb+Pb collisions at $\sqrt{s_{NN}} = 5.02$ TeV are collected. Thus with the

combination of RHIC and LHC, high quality data for heavy-ion collisions have now been available over quite a broad energy range. At the same time a large number of models have emerged which attempt to analyze and explain the data and extract physical parameters [6–10].

Global observables such as charged particle multiplicity distributions, pseudorapidity (η) distributions, momentum spectra, particle ratios, size of the fireball, and azimuthal anisotropy provide majority of the valuable information for thermal and chemical analysis of the freeze-out conditions [11, 12]. The η -distribution of charged particles is one of the most basic and most important observables to characterize the colliding system and to understand the phase transition. All the observables in heavy-ion collisions scale with the number of particles. So the knowledge of the particle density is essential for validating any measurement. The pseudorapidity particle density at mid-rapidity, along with transverse energy per particle provides the energy density of the fireball using the Bjorken estimation [13]. The pseudorapidity distributions are intimately connected to the energy density of the emitting source and provide an important test-bed for validating theoretical models, which attempt to describe the conditions in the early phases of the collision.

Experimental data for η -distributions have been reported for all the collider energies at RHIC [14, 15] and LHC [16–20]. In this article, we make a compilation of some of the available data in terms of the variation of pseudorapidity distributions of charged particles with beam energy and collision centrality. We

make a similar study using the string melting mode of the A Multi-Phase Transport (AMPT) model and make a comparison with the available data. In this model, different values of parton cross sections are used to explain the data at LHC. The pseudorapidity distributions, both from data and the AMPT model, of charged particles from $\sqrt{s_{\text{NN}}} = 7.7$ GeV to 2.76 TeV are fitted by a double Gaussian function. These parameters show interesting trends as a function of beam energy. Extrapolating the parameters to higher energies, we obtain the η -distribution for $\sqrt{s_{\text{NN}}} = 5.02$ TeV. It is observed that the pseudorapidity density at mid-rapidity matches well with the recently reported data from ALICE [21]. Furthermore, we extract the value of initial energy density for collisions at $\sqrt{s_{\text{NN}}} = 5.02$ TeV.

The paper is organized as follows. In Section II, we discuss the AMPT model which is used to compare the data results. In Section III, we present the compilation of pseudorapidity distributions for data and AMPT. In Section IV, we make an analysis of the shapes of the pseudorapidity distributions and present the results of the fit parameters. Energy dependence of charged particle multiplicity densities, pseudorapidity distributions and energy densities are presented. We conclude the paper with a summary in Section VI.

II. AMPT SETTINGS

The AMPT model [22] provides a framework to study relativistic heavy-ion collisions. It incorporates essential stages of heavy ion collisions from the initial condition to final observables on an event-by-event basis, including the parton cascade, hadronization and the hadron cascade [23–25]. The model can generate events in two different modes: (a) default, and (b) string melting (SM). Initial conditions for both the modes are taken from HIJING [26], where two Wood-Saxon type radial density profile are taken for colliding nuclei. The multiple scattering among the nucleons of two heavy ion nuclei are governed by the eikonal formalism. The particle production has two distinct sources, from hard and soft processes, depending on the momentum transfer among partons. In the default mode, energetic partons cascade through Zhang’s Parton Cascade (ZPC) before the strings and partons are recombined and the strings are fragmented via the Lund string fragmentation function,

$$f(z) \propto z^{-1}(1-z)^a \exp(-bm_T^2/z), \quad (1)$$

where a and b are the Lund string fragmentation function parameters, taken to be 0.2 and 2.2. ART (A Relativistic Transport model for hadrons) [27] is used to describe how the produced hadrons will

interact. In the String Melting mode, the strings produced from HIJING are decomposed into partons which are fed into the parton cascade along with the minijet partons. The partonic matter is then turned into hadrons through the coalescence model [28, 29] and the hadronic interactions are subsequently modeled using ART. The Default mode describes the evolution of collision in terms of strings and minijets followed by string fragmentation, and the String Melting mode includes a fully partonic QGP phase that hadronizes through quark coalescence.

In both the modes of AMPT, Boltzmann equations are solved using ZPC with total parton elastic scattering cross section,

$$\sigma_{gg} = \frac{9\pi\alpha_s^2}{2\mu^2} \frac{1}{1 + \mu^2/s} \approx \frac{9\pi\alpha_s^2}{2\mu^2}, \quad (2)$$

where α_s is the strong coupling constant, s, t are the Mandelstam variables and μ is the Debye screening mass. Here, α_s and μ are the key deciding factors for multiplicity yield at a particular centrality of given energy, and they are taken as 0.47 and 3.22, corresponding to $\sigma_{\text{gg}} = 10$ mb. For a beam energy range 7.7 GeV to 2.76 TeV we found global observables like pseudorapidity density [16], transverse momentum distribution [30], particle ratio [22], higher harmonic anisotropic flow [30] like v_2, v_3 are within the range of experimental error. We have carried out a comparison study for different observables by varying a, b, α_s and μ corresponding to 1.5 mb, 3 mb, 6 mb and 10 mb cross sections. The model therefore provides a convenient way to investigate expectations for a variety of observables with and without a QGP phase.

III. PSEUDORAPIDITY DISTRIBUTIONS - DATA AND AMPT

Pseudorapidity distributions of charged particles have been reported by fixed target as well as collider experiments. In this article, we concentrate on the results of collider experiments at RHIC and LHC. In Fig. 1, we present the experimental results from the PHOBOS experiment [14] at RHIC for central Au+Au collisions at $\sqrt{s_{\text{NN}}} = 19.6, 62.4$ and 200 GeV, and from the ALICE experiment [16] at LHC for Pb+Pb collisions at $\sqrt{s_{\text{NN}}} = 2.76$ TeV. It is observed that the distributions are symmetric around the mid-rapidity as they should be, but the dip structure at $\eta = 0$ gets more prominent with the increase of collision energy. For the LHC energy, the dip increases in going from peripheral to central collisions. The magnitude of the dip depends on the particle composition of the charged particles as the dip is more prominent for heavier particles like protons and anti-protons compared to pions.

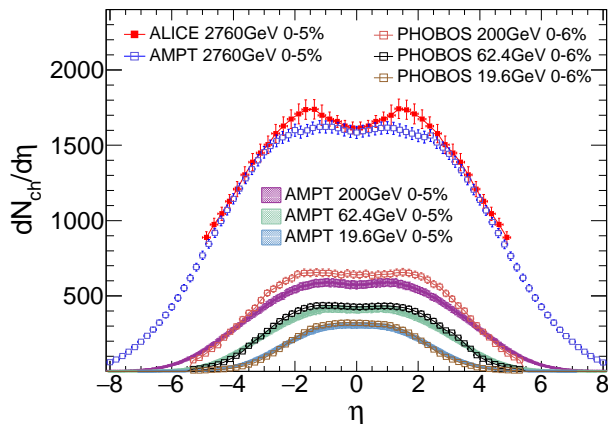


FIG. 1: Beam energy dependence of charged particle pseudorapidity distributions. Results from PHOBOS [14] and ALICE [16, 17] for central collisions are shown along with calculations from the string melting mode of AMPT model.

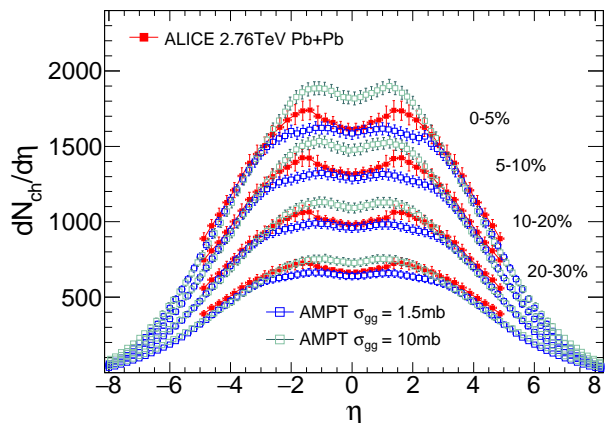


FIG. 2: Centrality dependence of charged particle pseudorapidity distributions for Pb+Pb collisions at $\sqrt{s_{NN}} = 2.76$ TeV with the data from ALICE experiment [16, 17] and those from the AMPT model for two settings of total parton scattering cross section (σ_{gg}).

In the present study, we have generated AMPT events with SM mode for different collision energies and collision centralities. The total parton elastic scattering cross section from 7.7 GeV to 200 GeV at RHIC energies is taken as $\sigma_{gg} = 10$ mb and for 2.76 TeV at LHC energy, it is chosen to be 1.5 mb. It is observed that with these settings AMPT can describe the data for transverse momentum spectra and flow [30]. The results of AMPT model calculations for η -distributions are superimposed on Fig. 1. The AMPT results describe the data at RHIC energy well. For $\sqrt{s_{NN}} = 2.76$ TeV, the data at mid-rapidity are well described by AMPT, but discrepancies are observed at other η -ranges especially at the peaks.

In Fig. 2, η -distributions for LHC data at $\sqrt{s_{NN}} = 2.76$ TeV for four centralities along with AMPT model data for two different parton scattering cross sections (1.5 mb and 10 mb) are shown. It is seen that the AMPT results with 1.5 mb matches the mid-rapidity value quite well. The distributions with 10 mb, match the shape of the data distribution very well, but miss the value at mid-rapidity. Henceforth, parton cross sections are kept at 1.5 mb for all calculations at LHC energies.

IV. SHAPES OF PSEUDORAPIDITY DISTRIBUTIONS

Further studies have been performed to investigate the centrality-wise variation of shape of the η -distributions for heavy-ion collisions, ranging from 7.7 GeV to 2.76 TeV. For central Au+Au collisions at RHIC energies, the distributions has been fitted by [32]:

$$\frac{dN_{ch}}{d\eta} = \frac{c\sqrt{1 - 1/(\alpha \cosh \eta)^2}}{1 + e^{(|\eta| - \beta)/a}}, \quad (3)$$

where a, c, α , and β are fit parameters.

Figures 1 and 2 show that the η -distributions exhibit double Gaussian nature, both for experimental data and AMPT. This double Gaussian nature is more prominent for higher collision energies and central collisions. The shapes can be represented by double Gaussian distributions of the form,

$$A_1 e^{-(\eta_1^2/2\sigma_1^2)} - A_2 e^{-(\eta_2^2/2\sigma_2^2)}, \quad (4)$$

where the fit parameters, A_1, A_2 are the amplitudes, η_1, η_2 are the peak positions, and σ_1, σ_2 are the widths of the two Gaussian distributions. The fit parameters represent the shapes of the distribution.

Both the experimental data and AMPT distributions are fitted with the double Gaussian functional form as above and the fit parameters are extracted. The fit parameters are presented in Fig. 3 as a function of collision energy for experimental data and AMPT calculations. All the errors shown in the this figure correspond to the error in fitting. The Gaussian fit parameters follow the following trends:

- (i) The normalization parameters, A_1 and A_2 increase with the increase of beam energy as per expectation. These parameters for available experimental data and AMPT are observed to be close together.
- (ii) The values of η_1 and η_2 represent the peak positions in the η distribution. As expected, η_1 and η_2 show opposite trends with the increase of the beam energy. This means that the peak positions in η spread out more with the increase of beam energy. It is to note that the values of η_1 and η_2 for data and AMPT are close together.

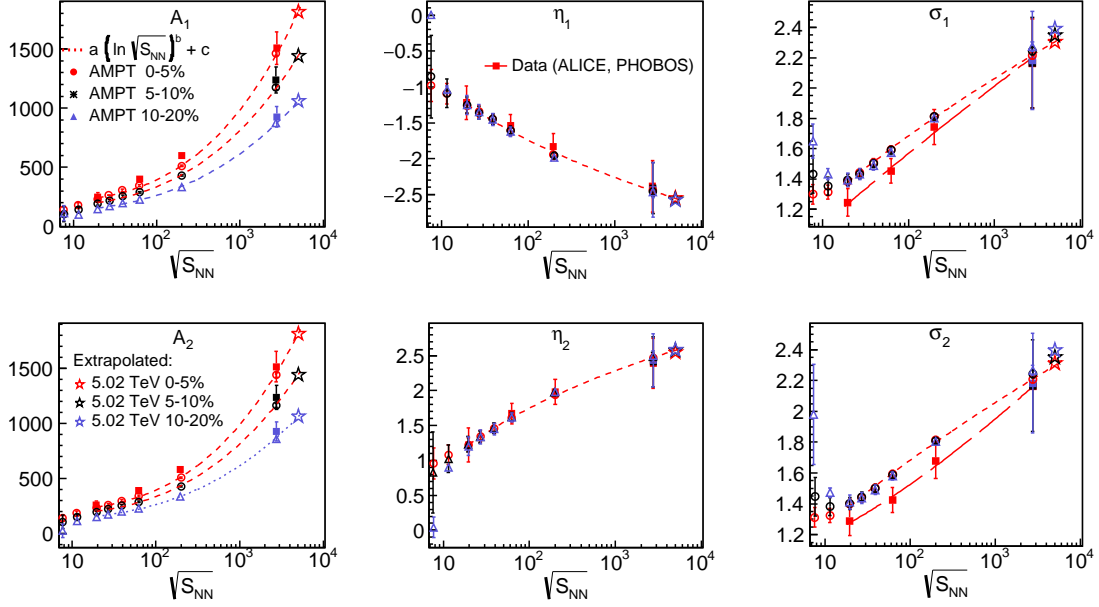


FIG. 3: Fit parameters of the double Gaussian fit to the η -distributions obtained from the AMPT model for Au+Au collisions from $\sqrt{s_{NN}} = 7.7$ GeV to 200 GeV and Pb+Pb collision at $\sqrt{s_{NN}} = 2.76$ TeV. Extrapolated values of the parameters for $\sqrt{s_{NN}} = 5.02$ TeV are also plotted in the figures.

TABLE I: Parameters of Double Gaussian fits to the η -distributions of Au+Au collisions from $\sqrt{s_{NN}} = 7.7$ GeV to 200 GeV, and Pb+Pb collisions at 2.76 TeV. Extrapolated parameters for $\sqrt{s_{NN}} = 5.02$ TeV are presented.

$\sqrt{s_{NN}}$ (GeV)	Centrality (%)	A_1	η_1	σ_1	A_2	η_2	σ_2
7.7	0-5	134.93 ± 25.67	-0.987 ± 0.223	1.294 ± 0.063	139.120 ± 25.05	0.225 ± 0.225	1.312 ± 0.064
	5-10	102.46 ± 63.61	-0.862 ± 0.576	1.432 ± 0.124	106.84 ± 62.43	0.825 ± 0.581	1.446 ± 0.126
	10-20	112.36 ± 61.54	-0.004 ± 0.047	1.648 ± 0.112	26.63 ± 61.93	0.042 ± 0.15	1.980 ± 0.325
11.5	0-5	178.72 ± 17.98	-1.097 ± 0.142	1.314 ± 0.045	180.78 ± 17.72	0.143 ± 0.143	1.323 ± 0.059
	5-10	142.25 ± 22.25	-1.091 ± 0.199	1.354 ± 0.059	150.42 ± 21.37	1.016 ± 0.199	1.380 ± 0.059
	10-20	100.56 ± 2.19	-1.037 ± 0.051	1.433 ± 0.035	114.22 ± 2.89	0.892 ± 0.037	1.473 ± 0.030
19.6	0-5	226.70 ± 13.19	-1.269 ± 0.098	1.383 ± 0.034	232.85 ± 12.90	1.223 ± 0.098	1.399 ± 0.034
	5-10	190.92 ± 12.63	-1.255 ± 0.111	1.392 ± 0.038	194.42 ± 12.44	1.224 ± 0.111	1.402 ± 0.038
	10-20	147.38 ± 11.90	-1.254 ± 0.132	1.393 ± 0.045	151.82 ± 11.58	1.203 ± 0.132	1.411 ± 0.045
27	0-5	260.45 ± 11.09	-1.344 ± 0.082	1.441 ± 0.029	260.59 ± 11.11	1.345 ± 0.082	1.441 ± 0.029
	5-10	218.19 ± 10.28	-1.361 ± 0.089	1.433 ± 0.032	221.92 ± 10.10	1.326 ± 0.089	1.446 ± 0.032
	10-20	171.77 ± 9.06	-1.346 ± 0.101	1.432 ± 0.036	172.96 ± 8.99	1.333 ± 0.100	1.437 ± 0.036
39	0-5	299.95 ± 9.79	-1.444 ± 0.069	1.508 ± 0.026	297.48 ± 9.87	1.457 ± 0.070	1.502 ± 0.026
	5-10	254.58 ± 8.83	-1.450 ± 0.074	1.501 ± 0.027	253.57 ± 8.87	1.455 ± 0.074	1.499 ± 0.027
	10-20	199.13 ± 7.64	-1.455 ± 0.082	1.490 ± 0.030	199.39 ± 7.62	1.450 ± 0.082	1.490 ± 0.031
62.4	0-5	341.36 ± 8.04	-1.605 ± 0.057	1.595 ± 0.022	340.53 ± 8.07	1.670 ± 0.057	1.594 ± 0.022
	5-10	288.93 ± 7.14	-1.608 ± 0.061	1.589 ± 0.023	287.59 ± 7.16	1.619 ± 0.061	1.587 ± 0.023
	10-20	225.61 ± 6.07	-1.625 ± 0.066	1.576 ± 0.026	225.71 ± 6.035	1.615 ± 0.067	1.580 ± 0.026
200	0-5	507.18 ± 6.81	-1.947 ± 0.041	1.812 ± 0.016	506.93 ± 6.77	1.940 ± 0.041	1.816 ± 0.016
	5-10	430.61 ± 5.97	-1.958 ± 0.043	1.813 ± 0.017	429.01 ± 5.99	1.965 ± 0.043	1.809 ± 0.017
	10-20	334.48 ± 4.97	-1.982 ± 0.047	1.804 ± 0.019	334.30 ± 4.97	1.979 ± 0.047	1.803 ± 0.019
2760	0-5	1458.69 ± 19.63	-2.442 ± 0.054	2.215 ± 0.022	1439.93 ± 19.75	2.471 ± 0.054	2.207 ± 0.022
	5-10	1174.33 ± 18.66	-2.462 ± 0.063	2.245 ± 0.026	1159.96 ± 18.68	2.475 ± 0.064	2.244 ± 0.026
	10-20	872.77 ± 16.66	-2.465 ± 0.075	2.274 ± 0.031	859.07 ± 16.63	2.493 ± 0.076	2.266 ± 0.032
5020 (extrapolated)	0-5	1814.52 ± 27.92	-2.554 ± 0.082	2.304 ± 0.039	1815.19 ± 28.00	2.549 ± 0.085	2.311 ± 0.040
	5-10	1441.13 ± 21.23	-2.573 ± 0.091	2.348 ± 0.046	1442.23 ± 22.80	2.579 ± 0.092	2.352 ± 0.050
	10-20	1059.63 ± 17.81	-2.575 ± 0.107	2.389 ± 0.051	1061.73 ± 18.10	2.585 ± 0.110	2.395 ± 0.050

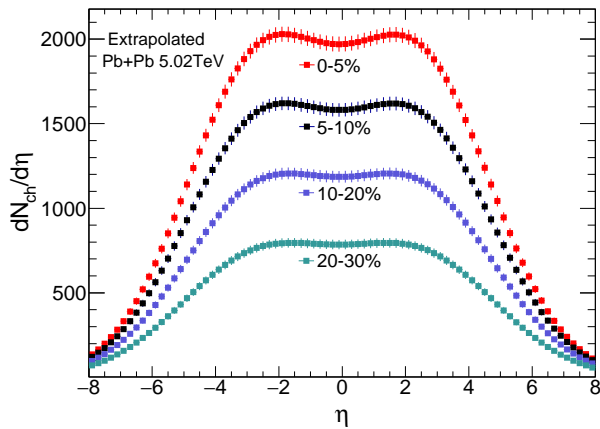


FIG. 4: η -distributions for Pb+Pb collisions at $\sqrt{s_{\text{NN}}} = 5.02$ TeV for different centralities. The distributions are obtained from the extrapolated AMPT parameters from lower energies.

(iii) The widths (σ_1 and σ_2), of the η -distributions increase as a function of beam energy. For lower collision energies, the widths extracted from data are smaller than those of AMPT, but are close together at higher energies.

From the comparison of the fit parameters for data and AMPT, we observe that the AMPT can be used as a proxy for experimental data. The AMPT points are fitted with power law fits, shown in Fig. 3 as dashed lines. These fit values provide a way to compute the η -distribution at any collision energy and centrality. Accordingly, these fit values are extended up to higher energy, *viz.*, $\sqrt{s_{\text{NN}}} = 5.02$ TeV. The Gaussian fit parameters, along with the extrapolated values for $\sqrt{s_{\text{NN}}} = 5.02$ TeV from AMPT are presented in Table I. With the extrapolated parameter set for Pb+Pb collisions at $\sqrt{s_{\text{NN}}} = 5.02$ TeV, the η -distributions at different collision energies are obtained. The results are shown in Fig. 4.

V. ENERGY DEPENDENCE OF GLOBAL PARAMETERS

Parameterization of η -distributions of charged particles from the AMPT model can be used to obtain energy dependence of several other global observables. Here we discuss the collision energy dependence of charged particle multiplicity density at mid-rapidity, centrality dependence of charged particle multiplicity density and the collision energy dependence of Bjorken energy density.

The quantity, $2(dN_{\text{ch}}/d\eta)/\langle N_{\text{part}} \rangle$, gives the charged particle multiplicity density at $\eta=0$ scaled by the average number of participant pairs ($\langle N_{\text{part}} \rangle/2$). Figure 5 shows the variation of this

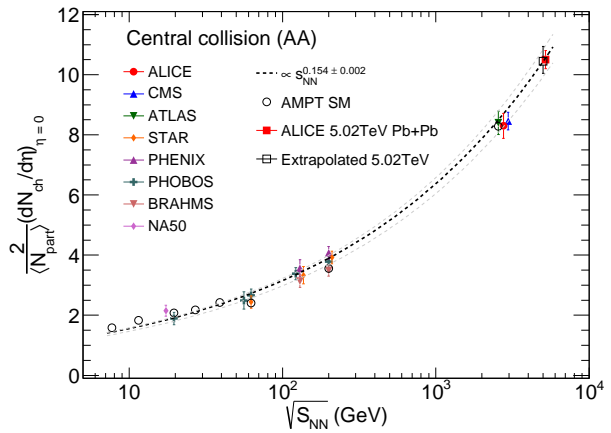


FIG. 5: Pseudorapidity density of charged particles, normalized to number of participant pairs ($\frac{2}{\langle N_{\text{part}} \rangle} (dN_{\text{ch}}/d\eta)_{\eta=0}$), plotted as a function of collision energy for central Au+Au or Pb+Pb collisions from experimental data and AMPT model. Some of the data points are shifted along x -axis for clarity of presentation.

quantity as a function of $\sqrt{s_{\text{NN}}}$ for central (top 5% cross section) collisions. The plot shows an increase in the multiplicity density with the increase of the collision energy. The data points are taken from PHOBOS, BRAHMS, STAR, and PHENIX experiments at RHIC and ALICE, CMS and ATLAS experiment at LHC. The results from AMPT model are shown by solid red points. For Pb+Pb data at 5.02 TeV, the extrapolated results from Fig. 4 have been plotted. The AMPT results explain the data quite well. A power law fit to the AMPT model data gives the fit value as $(0.77 \pm 0.04) s_{\text{NN}}^{0.154 \pm 0.002}$. This matches the fit given in Ref. [21]. As shown in the figure, the extrapolated value at $\sqrt{s_{\text{NN}}} = 5.02$ TeV is close to the recently published data from the ALICE experiment [21]. The beam energy dependence of charged particle multiplicity density has been studied for other centralities. Power law fit to each of the curves give the s_{NN} dependence as $s_{\text{NN}}^{0.154}$ to $s_{\text{NN}}^{0.109}$ from top central (0-5%) to peripheral (70-80%) collisions. This is consistent with the conclusion that the particle multiplicity increases faster for central collisions compared to peripheral collisions.

The centrality dependences of charged particle multiplicity density have been reported for Pb+Pb collisions at $\sqrt{s_{\text{NN}}} = 2.76$ TeV [16] and 5.02 TeV [21]. As discussed earlier, the AMPT model calculations describe the data well at $\sqrt{s_{\text{NN}}} = 2.76$ TeV. By extrapolating the fit parameters from the AMPT model to higher energies of $\sqrt{s_{\text{NN}}} = 5.02$ TeV, we obtain the centrality dependence of charged particle multiplicity density at this energy. For central (0-5%) collisions, the multiplicity density comes out to be 1964 ± 30 . The results from the ex-

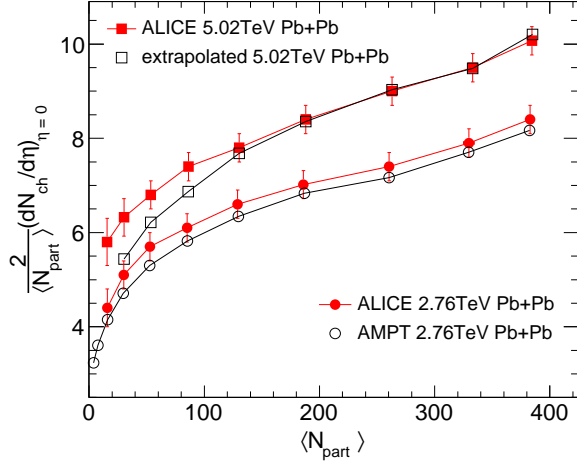


FIG. 6: Centrality dependence of $\frac{2}{\langle N_{\text{part}} \rangle} (dN_{\text{ch}}/d\eta)_{\eta=0}$ for Pb+Pb collisions at $\sqrt{s_{\text{NN}}} = 2.76$ and 5.02 TeV. AMPT model calculations for $\sqrt{s_{\text{NN}}} = 2.76$ TeV and extrapolations for $\sqrt{s_{\text{NN}}} = 5.02$ TeV reasonably explain the ALICE data [16, 21].

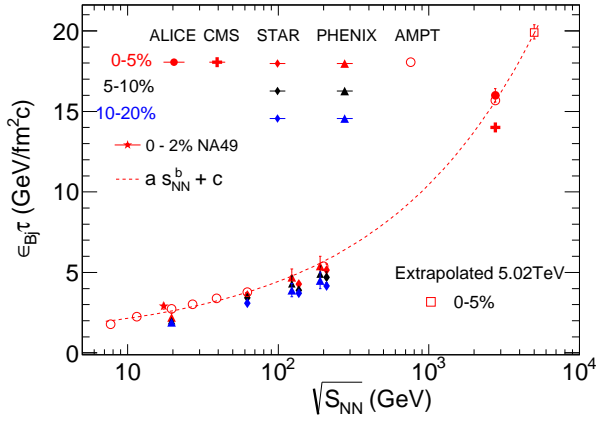


FIG. 7: Energy density ($\epsilon_{\text{Bj}}\tau$) as a function of $\sqrt{s_{\text{NN}}}$ for experimental data [15, 31–38] and AMPT model. Power law fits to the AMPT results are extrapolated to $\sqrt{s_{\text{NN}}} = 5.02$ TeV. Some of the data points are shifted along x -axis for clarity of presentation.

perimental data and AMPT calculations for both $\sqrt{s_{\text{NN}}} = 2.76$ and 5.02 TeV as a function of centrality are shown in Fig. 6. For Pb+Pb collisions at $\sqrt{s_{\text{NN}}} = 2.76$ TeV, the AMPT results are within the experimental errors. For Pb+Pb collisions at $\sqrt{s_{\text{NN}}} = 5.02$ TeV, the AMPT results agree with the experimental data points, except for peripheral collisions with $\langle N_{\text{part}} \rangle$ less than 130.

Charged particle multiplicity density is normally used to estimate the initial energy density of the

fireball by using the Bjorken estimation given as [13]:

$$\epsilon_{\text{Bj}} = \frac{1}{\pi R^2 \tau} \frac{dE_{\text{T}}}{dy}, \quad (5)$$

where τ is the formation time, πR^2 is the effective area of the fireball or the overlap area of the colliding nuclei, and dE_{T} is the total initial energy within a rapidity window dy . The last term can be approximated as [15]:

$$\frac{dE_{\text{T}}}{dy} \approx \frac{3}{2} \left(\langle m_{\text{T}} \rangle \frac{dN}{dy} \right)_{\pi^{\pm}} + 2 \left(\langle m_{\text{T}} \rangle \frac{dN}{dy} \right)_{K^{\pm}, p, \bar{p}}. \quad (6)$$

$\langle m_{\text{T}} \rangle$ is the mean transverse mass of identified particles (π^{\pm} , K^{\pm} , p or \bar{p}). The value of τ is typically taken as 1 fm. But in the absence of experimental knowledge of τ , the energy density is expressed in terms of $\epsilon_{\text{Bj}}\tau$.

The energy density, $\epsilon_{\text{Bj}}\tau$, as a function of collision energy is presented in Fig. 7 for experimental results at three centralities from NA49 [31], STAR [15, 33], PHENIX [32, 34, 35], ALICE [36, 37] and CMS [38] collaborations. In some cases, there are differences in experiments results at same collision energies show different results. AMPT model results are superimposed for central (0-5%) collisions. It is observed that the AMPT results reasonably describe the experimental data. The AMPT results of $\epsilon_{\text{Bj}}\tau$ are fitted with a power law (for central $\propto s_{\text{NN}}^{0.22 \pm 0.015}$) for different centralities. For central (0-5%) collisions, the value of $\epsilon_{\text{Bj}}\tau$ comes out to be 19.88 ± 0.48 GeV/fm²c. The value of the exponent in the power law fits are observed to vary from $s_{\text{NN}}^{0.22}$ to $s_{\text{NN}}^{0.10}$ for central (0-5%) to peripheral (70-80%) collisions, respectively. $\epsilon_{\text{Bj}}\tau$ is a combination of $dN_{\text{ch}}/d\eta$ and $\langle m_{\text{T}} \rangle$, both of which vary as power law with respect to collision energy. That may explain the origin of the power law behavior of energy density. As a function of collision energy, the energy density increases much faster for central collisions compared to peripheral collisions.

VI. SUMMARY

We have studied the η -distributions of produced charged particles for Au+Au collisions at $\sqrt{s_{\text{NN}}} = 7.7$ to 200 GeV, corresponding to the collisions at RHIC and for Pb+Pb collisions at $\sqrt{s_{\text{NN}}} = 2.76$ TeV, corresponding to the collisions at LHC. We have employed the string melting mode of the AMPT model to describe the experimental data. We observe that using the total parton elastic cross section, $\sigma_{\text{gg}} = 10$ mb, the AMPT model can explain the RHIC data, whereas $\sigma_{\text{gg}} = 1.5$ mb is needed for explaining the data at LHC. AMPT model, with these settings are used to further study

the η -distributions and initial energy densities. The shapes of the η -distributions could be explained by using double Gaussian functions with a set of parameters comprising of the amplitude, the position of the peaks in η , and the widths of the distributions. As expected, with the increase of the beam energy, the amplitudes increase, the peak positions move farther apart, and the widths of the distributions increase. The parameters are fitted well by power law fits, using which the pseudorapidity distributions can be obtained for any beam energy and collision centrality. We obtain initial energy density as a function of collision energy and collision centrality using Bjorken formalism. Power law fits to the multiplicity density at mid-rapidity give the s_{NN} dependence as $s_{NN}^{0.154}$ to $s_{NN}^{0.109}$ from top central (0-5%) to peripheral (70-80%) collisions. Similarly, power law fits to the energy density yield the s_{NN} dependence as $s_{NN}^{0.22}$ to $s_{NN}^{0.10}$ for the same centrality ranges. As a function of collision energy, the particle multiplicity and energy density increase much faster

for central collisions compared to the peripheral collisions. Extrapolating the parameters to collisions at $\sqrt{s_{NN}} = 5.02$ TeV, we are able to explain the recently published results on centrality dependence of charged particle multiplicity and energy density. At this energy, the pseudorapidity density of charged particles for central (0-5%) collisions is 1964 ± 30 and energy density, $\epsilon_{Bj} \tau$ is 19.98 GeV/fm²c. Furthermore, we note that the results obtained in the present study can be interpolated for intermediate energies to obtain η -distributions and energy densities for heavy-ion collisions in the Facility for Antiproton and Ion Research (FAIR). For laboratory energy of 11 GeV at FAIR, the energy density would be 1.8 GeV/fm³ for $\tau = 1$ fm, which is an interesting region to study the deconfined matter at high net-baryon density.

Acknowledgement This research used resources of the LHC grid computing centre at the Variable Energy Cyclotron Centre.

-
- [1] J.W. Harris, B. Muller, Ann. Rev. Nucl. Part. Sci. **46**, 71 (1996).
- [2] P. Braun-Munzinger and J. Stachel, Nature **448**, 302 (2007).
- [3] A. Bazavov *et al.* Phys. Rev. **D90**, 094503 (2014).
- [4] Y. Aoki *et al.* J. High Ene. Phys. **06**, 088 (2009).
- [5] M.M. Aggarwal *et al.* (STAR Collaboration) arXiv:1007.2613 [nucl-ex].
- [6] S. Ozonder, R.J. Fries, Phys. Rev. **C89**, 034902 (2014).
- [7] J. Dias de Deus and R. Ugoccioni, Phys. Lett. **B494** 53 (2000).
- [8] J. Zhi-jin and S. Yu-Fen, Chin. Phys. Lett. **29** 022502 (2012).
- [9] L. Zhou and G. Stephans, Phys. Rev. **C90**, 014902 (2014).
- [10] F.I. Shao, T. Yao and Q. Xie, Phys. Rev. **75**, 034904 (2007).
- [11] M. Kliemant, R. Sahoo, T. Schuster and R. Stock, The Physics of the Quark-Gluon Plasma, Vol. 785 of the series Lecture Notes in Physics pp 23-103, Springer Publication.
- [12] R. Sahoo, A.N. Mishra, N.K. Behera, B.K. Nandi, Adv. in High Ener. Phys., **2015** (2015).
- [13] J.D. Bjorken, Phys. Rev. **D27**, 140 (1983).
- [14] B. Alver *et al.* (PHOBOS Collaboration), Phys. Rev. **C83**, 024913 (2011).
- [15] B.Abelev *et al.* (STAR Collaboration), Phys. Rev. C **79**, 034909 (2009).
- [16] E. Abbas *et al.* (ALICE Collaboration), Phys. Lett. **B726**, 610 (2013).
- [17] J. Adam *et al.* (ALICE Collaboration), arXiv:1509.07299 [nucl-ex].
- [18] Y. Chen *et al.* (ATLAS Collaboration), J. Phys. **G38**, 124042 (2011).
- [19] G. Aad *et al.* (ATLAS Collaboration), Phys. Lett. **B710**, 363 (2012).
- [20] S. Chatrchyan *et al.* (CMS Collaboration), Jour. High Ene. Phys. **1108**, 141 (2011).
- [21] J. Adam *et al.* (ALICE Collaboration), arXiv:1512.06104 [nucl-ex].
- [22] Z.W. Lin, C.M. Ko, B.A. Li, B. Zhang, S. Pal, Phys. Rev. **C72**, 064901 (2005).
- [23] Z.W. Lin, arXiv:1403.1854 [nucl-th].
- [24] S. Pal and M. Bleicher, Phys. Lett. **B709**, 82 (2012).
- [25] J. Xu and C.M. Ko, Phys. Rev. **84**, 014903 (2011).
- [26] X.-N. Wang, M. Gyulassy, Phys. Rev. **D44**, 3501 (1991).
- [27] B. Li, A. T. Sustich, B. Zhang and C. M. Ko, Int. J. Mod. Phys. **E10**, 267 (2001)
- [28] R.J. Fries, V. Greco, P. Sorensen, Ann. Rev. Nucl. Part. Sci. **58**, 177 (2008)
- [29] R. J. Fries, B. Muller, C. Nonaka, S.A. Bass, Phys. Rev. Lett. **90**, 202303 (2003)
- [30] D. Solanki, P. Sorensen, S. Basu, R. Raniwala, and T.K. Nayak, Phys. Lett. **B720**, 352 (2013).
- [31] T. Alber *et al.*, Phys. Rev. Lett. **75**, 3814 (1995).
- [32] K. Adcox *et al.* (PHENIX Collaboration), Phys. Rev. Lett. **87**, 052301 (2001).
- [33] J. Adam *et al.* (STAR Collaboration), Phys. Rev. C **70**, 054907 (2004).
- [34] S.S. Adler *et al.*, (PHENIX Collaboration), Phys. Rev. **C71**, 034908 (2005).
- [35] J.T. Mitchell *et al.*, (PHENIX Collaboration), arXiv:1601.00904 [nucl-ex].
- [36] C. Loizides *et al.* (ALICE Collaboration), Jour. Phys. **G38**, 124040 (2011).
- [37] A. Toia *et al.* (ALICE Collaboration), Jour. Phys. **G38**, 124007 (2011).
- [38] S. Chatrchyan *et al.* (CMS Collaboration), Phys. Rev. Lett. **109**, 152303 (2012).